14

A Global View of Dispersion above the Mid-ocean Ridge

K.G. SPEER, M.E. MALTRUD, and A.M. THURNHERR

Department of Oceanography, Florida State University,
Tallahassee, FL 32306–4320, U.S.A.

ABSTRACT

The products of hydrothermal circulation are dispersed in the ocean by the crest-depth currents near mid-ocean ridges. Depending on the characteristics of the flows, dispersal can be governed by advective or diffusive laws. Statistical estimates of dispersion generally require Lagrangian observations, usually in the form of drifter trajectories. Only a few instances of these exist at the mid-ocean ridge, so global dispersion characteristics are deduced from a numerical simulation of ocean circulation. Initial tracer positions were distributed at 30–100 km spacing 200 m above the crest of the entire mid-ocean ridge. Trajectories were calculated for a 10-year integration period, and a subsample of about 1000 trajectories is used here. Various mechanisms are responsible for dispersion; a basic description and simple quantification of dispersion is presented. Away from the circumpolar current and the subpolar northwestern Atlantic, the greatest zonal dispersion occurs within 10° of the equator while the smallest dispersal is observed in the northeastern Pacific near the eastern boundary. Using typical deep-ocean values, it is shown that off-axis advection is initially set by turbulent diffusion, but that after a time of the order of months to years the transport is set by the mean velocity.

INTRODUCTION

Physical, chemical, and biological tracers of ocean circulation are generated at mid-ocean ridges (MORs) by a variety of mechanisms. These include geothermal heating, which modifies the temperature–salinity relationship of deep water, water–rock interactions, which supply various chemicals, and the colonization of the seafloor by organisms. The latter release larvae in diverse forms into ambient currents as a kind of biological tracer. Both the chemical and biological tracers can be nonconservative in the sense that they change form or perish after some period of time. The time scales for such change are only partially understood;

Energy and Mass Transfer in Marine Hydrothermal Systems
Edited by P.E. Halbach, V. Tunnicliffe, and J.R. Hein

however, the simple fact that chemical reactions and decomposition take place implies that chemical and biological tracers will interact with the ocean circulation in ways that lead to complex dispersal patterns. Even conservative tracers that are advected away from their sources without change can have complicated dispersal properties, depending on the nature of the ocean circulation in a given region of the ridge.

The deep ocean circulation near the MOR is mainly driven by wind and thermohaline forcing (heat and freshwater fluxes) at the surface of the ocean. These mechanisms set up the basic structure of ocean gyres, boundary currents, and the Antarctic Circumpolar Current that dominate large-scale maps of mean flows and variability, or eddy currents. A host of intermediate-scale phenomena exist to drive flow as well, from mesoscale turbulence to rectified tidal flow. The buoyancy fluxes associated with hydrothermal vent fields force motions on a wide range of scales, including convective plumes, rotationally driven secondary circulations, and even basin-scale flows (see reviews by Helfrich and Speer 1995; Lupton 1995; McDuff 1995; Speer and Helfrich 1995).

The ridge itself produces a very strong organizing effect on flow near the crest and above the flanks. Seafloor topography has spatial scales from grains of sand to the planetary scale exerting some control over flow. Examples of control include the geometry of ocean basins, sills, and passages and, on the smallest scales, the drag induced by bottom roughness. However, the topography of the ridge not only constrains flow kinematically to be along walls and within canyons, but also provides for new kinds of motion both locally, as in hydraulic flow over sills and topographic waves, and on segment and larger scales in the form of lee waves and other stationary or steady flows locked to the structure of the underlying topography. On large scales in the interior of ocean basins the flow tends to follow geostrophic contours, that is, contours of $\sin(\varphi)/H$, where φ denotes latitude and H is the ocean depth (LaCasce and Speer 1999; LaCasce 2000).

In the context of dispersal of hydrothermal tracers, it is sometimes useful to distinguish between along-ridge flows and cross-axis flows, retaining the tracers near the ridge system and dispersing them into the deep ocean basins, respectively. Is it possible to separate the diverse mechanisms responsible for deep flow into those which tend to force flow along the ridge and those which tend to force cross-ridge flow? This is not a physically meaningful separation since any variation in forcing along the ridge will set up cross-ridge flow. Still, to a certain extent, one can consider that the wind-driven flow often tends to carry fluid away from the ridge while the thermohaline flow often forms deep boundary currents that flow along the ridge. As shall be seen, this division holds in a limited sense at lower latitudes where relatively strong wind-driven equatorial waves appear to be responsible for much of the observed zonal (i.e., cross-axial) flow at mid-depths (MOR crest levels). At all latitudes, though, thermohaline flows may be part of the zonal flow carrying fluid away from the ridge; the flow through the Romanche and Chain Fracture Zones (FZs) along the equator in the Atlantic Ocean is a well-documented example (Mercier and Speer 1998). A recent experiment, including purposefully released tracer specifically designed to measure tracer advection and diapycnal diffusion on the flank of the Mid-Atlantic Ridge (MAR) at about 19°S, has revealed enhanced levels of vertical mixing over the rough topography (Polzin et al. 1997). Repeat observations of the tracer distribution as it evolves over the flank show flow paths along the flank as well as across the ridge axis through a nearby FZ (Ledwell, pers. comm.), i.e., the detailed structure of the ridge controls basic aspects of the ocean circulation.

The distributions of naturally occurring hydrothermal tracers have been a great source of information about the deep circulation, especially in the South Pacific. There, the original measurements of Lupton and Craig (1981), showing a large-scale westward-pointing plume of excess helium near 15°S, and those of Klinkhammer and Hudson (1986), showing eastward drift farther south, have been augmented over the years by other tracers and further observations of helium (WOCE, HELIOS). The HELIOS data set from the southern East Pacific Rise (EPR) includes direct velocity measurements with neutrally buoyant floats, and has lead to more quantitative estimates of flow and mixing near the ridge (Hautala and Riser 1993). Recent WOCE measurements in the South Atlantic have revealed hydrothermal helium anomalies emanating from the crest of the MAR as well (Rüth et al. 2000). In contrast to the Pacific plumes, the hydrothermal helium distribution in the South Atlantic is much more symmetric about the ridge crest, extending several hundreds of kilometers over the flanks on both sides, suggesting a diffusive (random walk) dispersal process, as opposed to simple advection by a mean flow. In a regional study Baker et al. (1985) observed effective off-axis transport of suspended particles at a site where the mean flow was predominantly along axis, again suggesting a significant turbulent-diffusive contribution to dispersal.

In the analysis of turbulent flows, the velocity fields are often separated into mean and fluctuating components (Reynolds decomposition), both of which advect passive tracers. The fluctuating components tend to disperse particles starting at nearby locations or in the same place at different times. Because of statistical similarities with molecular diffusion dispersion caused by turbulent flows is commonly called eddy or turbulent diffusion. As will be seen realistic evaluation of dispersion in the ocean requires observations of spreading tracers or flow trajectories (Lagrangian data), and there are almost none near the MOR system. In this chapter, we discuss dispersion near the MOR in the three major ocean basins using a global numerical simulation of ocean circulation. This is not meant to be a synthesis of dispersion mechanisms, of which there are many operating in the numerical model, nor do we try to evaluate the data from particular sites, like the Juan de Fuca Ridge, which have a history of flow observations. Finally, our simulated trajectories come from a numerical model that cannot resolve small-scale flow within rift valleys and other canyons on the ridge. We are concerned here only with the larger-scale dispersal once particles have escaped the canyons.

Eulerian and Lagrangian Approaches

Eulerian measurements are made at a fixed point $\mathbf{x}$ in space, for example, of velocity $u(x,t)$ by a moored current meter. Lagrangian measurements are time series of tracer positions, for example, the geographic locations of a float $x(t)$. Lagrangian measurements can be differentiated in time to get velocities following the flow. Typically, Eulerian velocity is averaged in time to produce a record mean flow; it is possible to average Lagrangian velocities of drifters passing through a given area to produce a corresponding mean. This is not the only way to define a Lagrangian mean, and there are various issues related to real, finite sampling by a limited number of drifters that need to be taken into account when estimating Lagrangian statistics (Davis 1991).

In unsteady flows, Eulerian and Lagrangian means at the same point are often different, as illustrated by the example of Stokes drift associated with a train of idealized surface-gravity waves in Figure 14.1. The solid circle shows the integrated Eulerian velocities, which have a

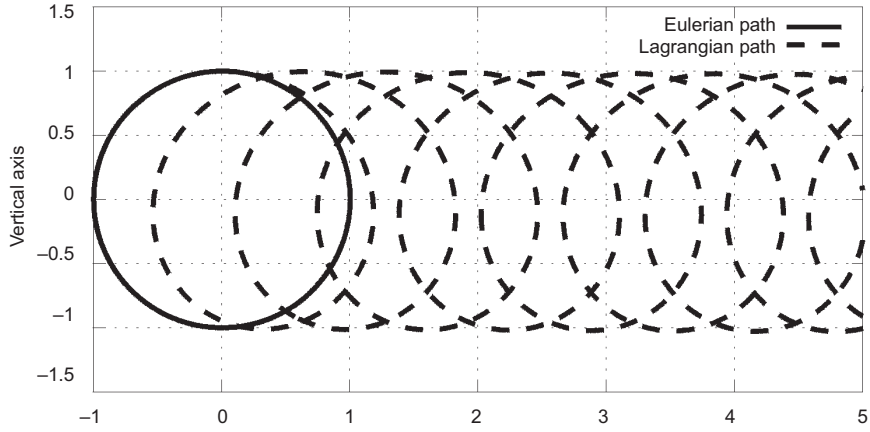

Figure 14.1 Hodographs (integrated velocity measurements) of Eulerian (solid) and Lagrangian (dashed) velocities under a train of idealized surface gravity waves propagating to the right.

zero mean value. The dashed line shows the corresponding integrated Lagrangian velocities illustrating a horizontal mean velocity in the direction of wave propagation. This Stokes drift is caused by the exponential dropoff of the velocities with depth, i.e., the positive horizontal velocities associated with the wave crests are always greater than the negative velocities in the deeper troughs. Stokes drift is not restricted to surface gravity waves but is a common feature of unsteady flows.

With a data set of Lagrangian measurements in hand, dispersion is usually calculated as

$$d^2 = < \left(x(t) - x(t_0) - < x(t) - x(t_0) > \right)^2 >, \tag{14.1}$$

where t_0 is the time of tracer release and the brackets denote ensemble averages over the available trajectories. Subtraction of the initial position and of the cluster mean position at time t before averaging implies that d^2 is a measure of the area covered by a set of tracers, i.e., it does not include the effect of the advection of the entire cluster by the time-averaged flow.

Even in situations where the flow is nearly steady, so that Lagrangian means are not significantly different from Eulerian means, it is often impractical to obtain sufficient sampling over an area of interest to determine the full range of spatial scales relevant for dispersal. Limited information about the dispersal capability of a flow field is extractable from an array of Eulerian current meters when that field varies significantly with position. An example of this situation is shown in the left panel of Figure 14.2, where the dominant flow in the rift valley of the MAR near 36°N is northeast across a sill separating two deep basins (Thurnherr et al. 2002). After the water crosses the sill, it turns to follow the bathymetry, flowing around the "rim" of the basin near sill depth; several instruments recorded this flow. Obviously, estimates of dispersion from instruments placed at different locations within the flow will show quite different results, and one way to illustrate this is with a hodograph (displacement from time integration of the measured velocity field, also called progressive-vector diagram).

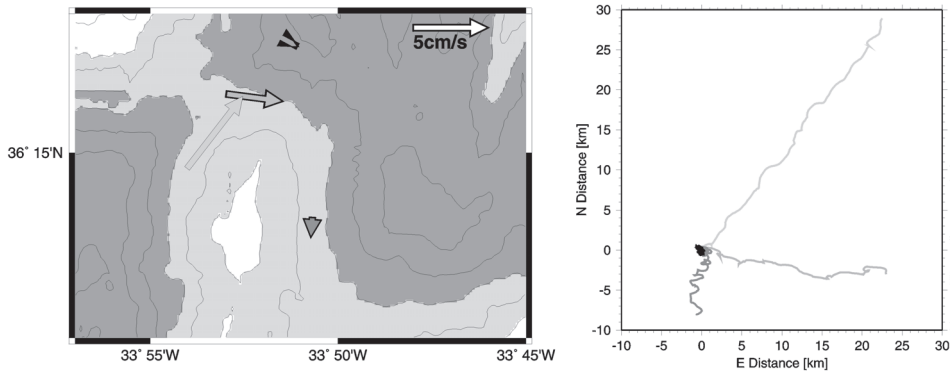

Figure 14.2 Current-meter measurements at 2100 m in the rift valley of the mid-ocean ridge. Left panel: bathymetry (depths below 2000 m are shaded; contour interval is 250 m) and one-week mean flow velocities. Right panel: hodographs over the same period; grayscale matches the shading of the arrows in the left panel.

Three instruments near the sill show nearly steady, opposing flows (right panel). If we were to assume that the Eulerian measurements represent Lagrangian trajectories and estimated dispersion, for example, using Equation 14.1, the result would be meaningless because velocity varies on small spatial scales, which is commonly the case near topography, even if the measurements are taken at some distance above the shallowest point.

Lagrangian Observations near Mid-ocean Ridges

The HELIOS experiment combined hydrographic measurements, tracer observations, and Lagrangian drifter trajectories to investigate the westward penetration of the South Pacific helium plume discovered by Lupton and Craig (1981). The float observations (see Figure 14 in Hautala and Riser 1993) led to a better description of the large-scale circulation, but were not designed to quantify dispersion from the crest of the EPR.

A direct, Lagrangian observation of flow connected to hydrothermal activity at a ridge crest was made by Lupton et al. (1998), who launched a neutrally buoyant float into a large event plume above the Gorda Ridge in the northeast Pacific (left panel of Figure 14.3). The trajectory is consistent with one that would result from an anticyclonically rotating mass of plume fluid (right panel) drifting westward in the absence of background flow. In terms of dispersion this trajectory is special, since the float was placed purposefully in the plume in order to track it, so the trajectory does not represent the average motion of water in this region. Many more trajectories from the surrounding environment and from plumes would be needed to construct significant flow statistics.

Another example of directly measured flow near the MOR using Lagrangian techniques comes from the Eurofloat experiment (Speer et al. 1999). This experiment was designed to observe the flow of Labrador Sea Water at a depth of 1750 m in the eastern basin of the North Atlantic (Figure 14.4). A number of floats were placed above the ridge (near crest levels), north of the Azores Plateau, since this was a potential pathway for the deep water to flow south from its region of formation in the Labrador Sea. A relatively strong (several cm/s)

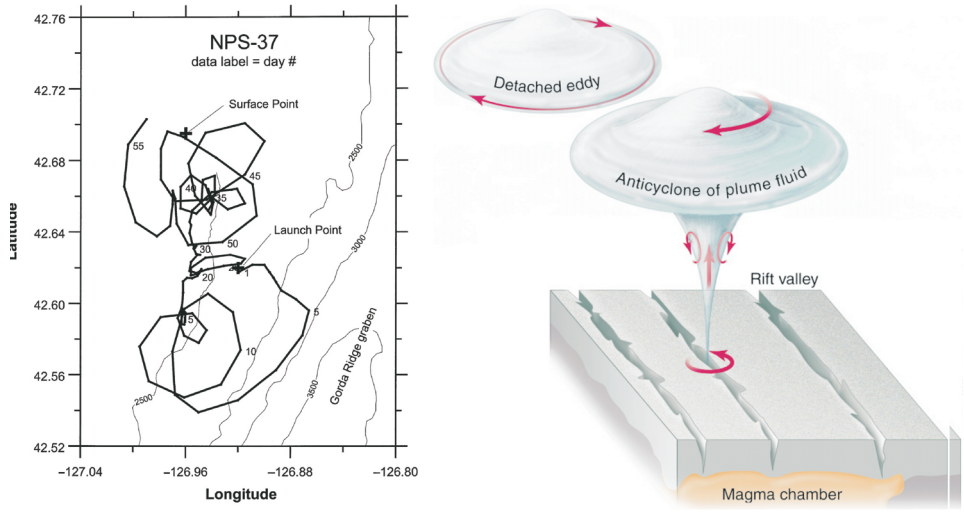

Figure 14.3 A two-month drifter trajectory near the crest of the Gorda Ridge (left, from Lupton et al. 1998). Schematic diagram of the rotating eddy generated by a plume of buoyant hydrothermal fluid released at the crest of the mid-ocean ridge (right, from Speer 1998).

current was found on the eastern flank of the ridge, carrying deep water around the plateau from north to south. After four years, a few trajectories suggest that the flow continues to the west across the MAR through the Oceanographer FZ at 35°N. This is a good example of the different circulation regimes that can be found at the MOR, with strong along-ridge transport in one area and cross-ridge flow in another. North of the Azores plateau, near 44°N, two floats can be found close to the ridge axis and one appears to have followed the rift valley northward

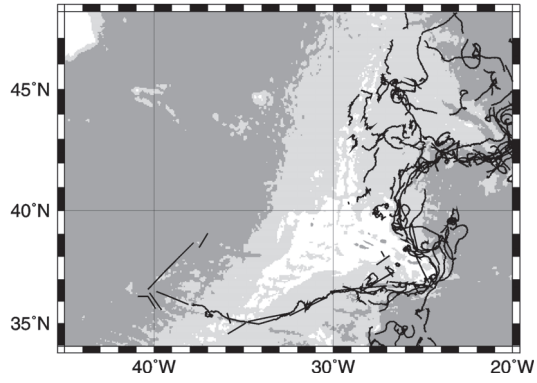

Figure 14.4 Trajectories from a Lagrangian experiment in the northeastern Atlantic Ocean. The experiment is ongoing; results from those instruments deployed near the Azores Plateau are shown and represent four years of drifting at 1750 m depth. Bathymetry below 2000 m is shaded; islands and depths below 3500 m are shown in dark gray. Float positions are plotted daily; acoustic tracking was not always available and in those cases net displacement over a cycling period of three months are displayed (straight-line segments).

for at least 100 km before crossing the crest and returning southward on the western flank. This experiment is ongoing and longer trajectories will eventually sample more of the ridge, though at decreasing spatial coverage as the instruments disperse.

These examples show how far we are from a complete description of the dispersal properties near the MOR as a whole. Transport within the rift valley might be quite different from that outside the valley, either above it or over the flanks of the ridge on either side (e.g., Thurnherr et al. 2002). Larger-scale flow structures, such as around the Azores Plateau, may be controlling the overall dispersion on time scales of a few years or more, while very different mechanisms may be responsible for the transport at small spatial and temporal scales.

SIMULATED FLOW TRAJECTORIES

As a first step in the development of a comprehensive simplified model for the dispersion of tracers on the ridge, Lagrangian motion can be examined in the framework of a global numerical simulation of ocean circulation, with realistic geometry, forcing, and high spatial and temporal resolution. Every general circulation model is a compromise between resolution and computing power; more resolution usually brings with it more physical phenomena and a better representation of previously resolved phenomena. The model used here (see appendix) is one of the highest resolution global numerical experiments achieved to date. Different dispersion regimes will be identified and estimates of dispersion will be presented.

Drifters were deployed in the model within 200 m of the bottom along the ridge crest. The results presented here are based on 10-year drifter trajectories, stored at 10-day intervals. For presentation, the trajectories were divided into regional boxes focusing on the ridge crest in the major ocean basins. The Southern Ocean requires a somewhat different analysis, since trajectories show large vertical excursions, and is being investigated separately.

Atlantic Ocean

The northern part of the North Atlantic is a region of vigorous deep water formation and the circulation near the MAR as indicated by float trajectories reflects that activity (Figure 14.5, left panel). The Denmark Strait outflow and the spreading of Labrador Sea Water, in particular, give rise to strong currents in the western basin north of approximately 30°N. Between 10° and 30°N the floats remain in a relatively narrow meridional band slightly west of the ridge crest while there is coherent westward flow towards the south American continent between 7° and 10°. The flow around the Azores Plateau is highly organized and carries floats over great along-ridge distances, similar to the observations (Figure 14.4), though at reduced strength. This is a typical problem with the deep flow in numerical simulations; away from the strong major surface currents, the model circulation tends to be too weak. Nevertheless, the model does appear to reproduce correctly many aspects of the flow, where comparison with data is possible. More detailed comparisons using model and drifter data from the Atlantic are underway.

In the South Atlantic, a basic division of flow into equatorial and higher latitude regimes becomes apparent (Figure 14.5, right panel). Within about 5° of the equator, strong, deep, zonal flow caused by equatorial Rossby waves carries drifters back and forth over several

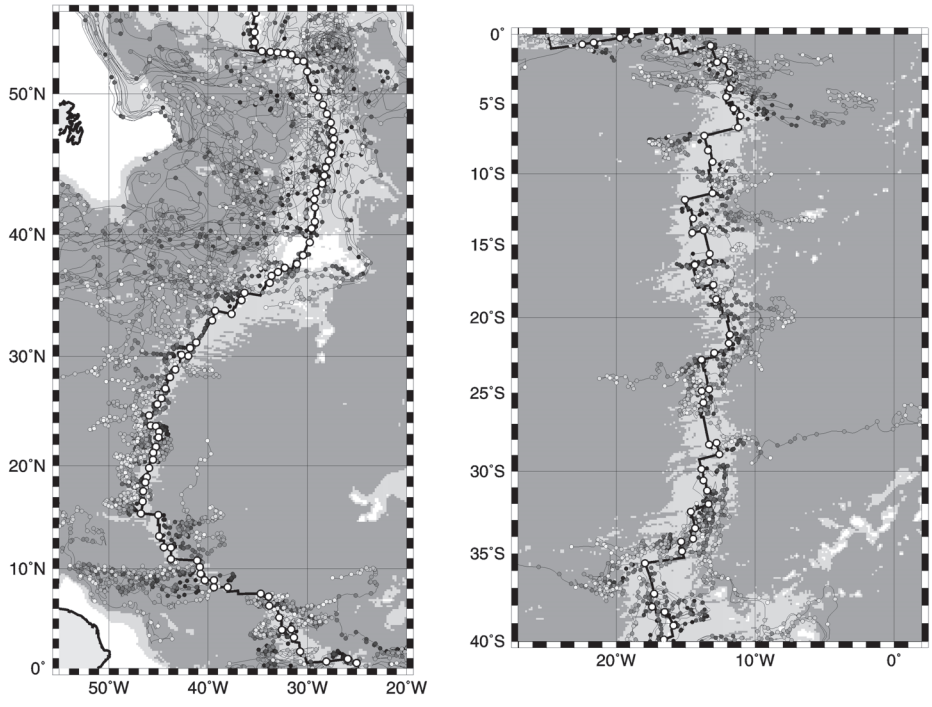

Figure 14.5 Simulated float trajectories at crest depth near the MAR (left panel: North Atlantic; right panel: South Atlantic); thick solid lines indicate ridge axis; bathymetric shading increases at 2000 m and 3500 m. The initial position of each trajectory is 200 m above the crest on the ridge axis (open white circles); filled circles mark 100-day intervals and lighten from black to white over the 10-years duration.

hundreds of kilometers. The seasonal signal is strongest, but other components with periods up to three years or so are also significant. Maximum zonal speeds are of order 20 cm/s in this region, and mean speeds are several centimeters per second over 1–2 year subsamples of the ten-year record. At higher latitudes the zonal velocity drops by nearly an order of magnitude, and the frequencies of the main energetic velocity components are lower, with corresponding periods of 1–2 years or more. There are along-slope as well as cross-slope aspects to the model flow with a tendency of the trajectories to follow the bathymetric structure of the ridge. Near major FZs, such as at 7°S (Ascension FZ), 17°S (Bagration FZ), and 23°S (Rio de Janeiro FZ), the drifter trajectories are predominantly parallel to the strike of the fractures. In a meridional sense the floats tend to follow the large-scale shape of the ridge (e.g., between 18°S and 25°S). Between 5°S and 40°S only a few trajectories show substantial off-axis displacements on either side of the ridge during the ten-year integration. The few excursions that do exist in this region are thought to be caused mainly by deep expressions of the wind-driven flow, with the exception of a zonal jet near 20°–25°S (Treguier et al., **in preparation**). South of 40°S the flow becomes zonal and consistently eastward in the Antarctic Circumpolar Current.

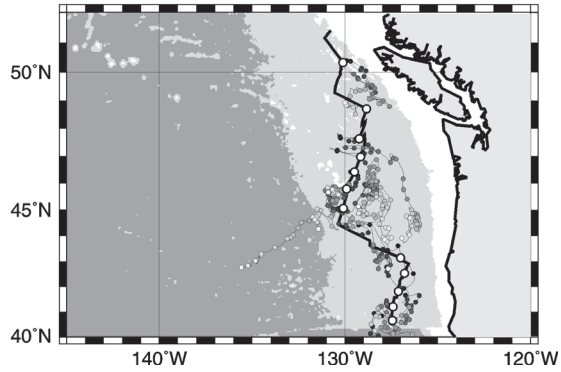

Figure 14.6 Simulated trajectories in the northeastern Pacific Ocean. See Figure 14.5 for shading and symbols.

Pacific Ocean

The MOR in the eastern North Pacific runs into the north American continent, which blocks zonal dispersion in two ways: kinematically, as a solid barrier to eastward flow, and dynamically, since idealized models of the large-scale ocean circulation show zonal flow building from east to west, with the strongest flow near the western boundary. Therefore, westward dispersion is expected to be strongly reduced near the eastern boundary. Indeed, trajectories from the northeast Pacific (Figure 14.6) show limited zonal penetration, except for a single trajectory characterized by a consistent southwestward drift of approximately 0.5 cm/s during four years. This does not mean that zonal dispersion does not take place, only that it takes longer than elsewhere. This particular trajectory exhibited a vertical excursion of about 400 m to 1500–1600 m where it catches a southwestward current after about two weeks.

In the equatorial region of the EPR (Figure 14.7), the strong influence of deep-reaching equatorial Rossby waves, forced by the wind at the surface, is again visible, roughly between 5°N and 5°S. This is the latitude band for which zonal dispersion is maximal. Near 10°N, coherent westward drift is evident as well as a few trajectories near 15°N that are apparently caught up in the flow associated with tropical instabilities of the surface currents at these latitudes. These trajectories are longer and make broad loops. South of the equatorial region, the trajectories show a rather simple large-scale pattern, with dominantly westward flow between 15°S and 25°S, and eastward motion south of 28°S. The eastward motion near 30°S is presumably connected to the complex shape of the intersecting ridges. Farther south, off-axis flow is limited, until the Antarctic Circumpolar Current is reached and very strong eastward flow occurs (not shown). South of 15°S the circulation pattern agrees with the large-scale hydrothermal tracer distributions and is roughly consistent with Reid's (1986) presentation of deep flow in the South Pacific; however, the model indicates a much richer structure to deep flow than the broad, simplified structure of Reid's analysis.

Indian Ocean

The circulation near the ridge system in the Indian Ocean is markedly different from that of the South Pacific and South Atlantic (Figure 14.8). Both the long South Atlantic and South

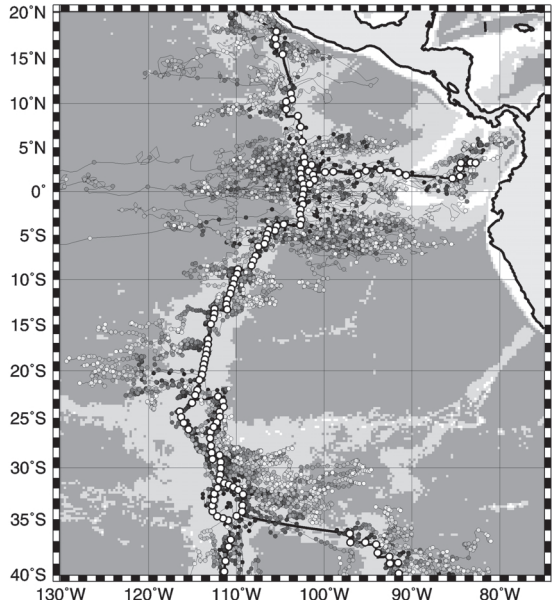

Figure 14.7 Simulated trajectories near the East Pacific Rise. See Figure 14.5 for shading and symbols.

Pacific ridges are separated zonally from other bathymetric highs of significant meridional extent while the Central Indian Ridge is partially bracketed on both sides. Thus, the near-ridge flow north of 20°S tends to be zonally trapped almost everywhere. Similar to the Atlantic and the Pacific cases, there is enhanced zonal dispersion near the equator, although in this case it is partially restricted by the topography. Between 20°S and 35°S, the near-axial flow is largely crest parallel. South of 35°S, the trajectories show westward flow across the Crozet Basin from the Southeast Indian Ridge to the Southwest Indian Ridge. This flow is consistent with Stramma's (1992) description of recirculation north of the South Indian Ocean Current, the principal current associated with, but somewhat north of the Subtropical Front in the southern Indian Ocean. South of 45°S (not shown), the frontal zones of the Antarctic Circumpolar Current begin, and deep flow is eastward.

DISPERSION AND DIFFUSION

There are various ways to reduce and quantify Lagrangian trajectory data, and choices are made based on the desired goals. For this discussion, we have chosen the key issue of the rate of zonal (i.e., off-axis) dispersion over different portions of the ridge. Where is this strong or weak, and how quickly do tracers move away from the crest? Along-ridge dispersion is obviously important as well, but more complicated, since very different flow regimes are encountered at different depths on the flank. We restrict discussion here to the off-ridge component. A statistic which quantifies the off-ridge dispersion is the root mean square (RMS) zonal displacement, shown for all three major ocean basins averaged in 5°-latitude bins between 40°S and 50°N in Figure 14.9. Consistent with the qualitative analysis of the float trajectories, the

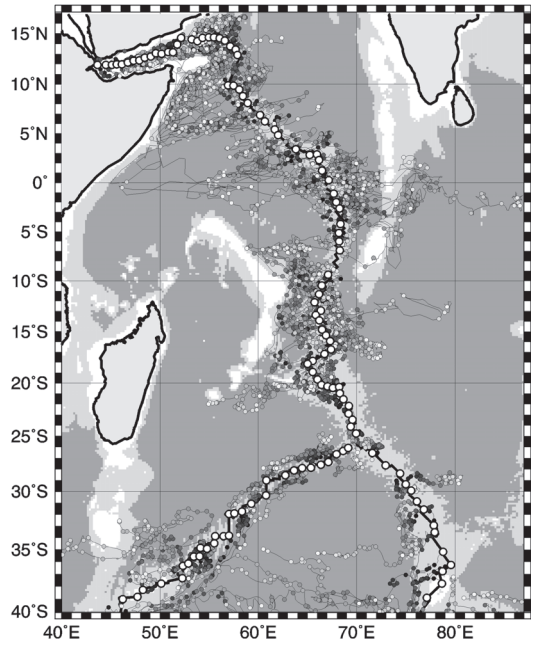

Figure 14.8 Simulated trajectories near the Central Indian Ridge and the Indian Ocean Triple Junction. See Figure 14.5 for shading and symbols.

maximal zonal dispersal between 30°N and 30°S takes place near the equator and attains minima at approximately ±20° degrees latitude. The smallest values in the regions considered are found in the northeast Pacific near the eastern boundary and the largest ones are found in regions of significant mean flows in the subpolar North Atlantic and the southern Indian Ocean. In a wide latitudinal band, the zonal dispersion from the EPR is significantly greater than that in the Atlantic and in the Indian Ocean. Zonal dispersion in the South Atlantic in particular is relatively uniform and small between 10°S and 35°S, i.e., over the entire region of the helium plume shown by Rüth et al. (2000). Plots of maximal RMS zonal excursion in 5°-latitude bins are similar in shape to ones shown but approximately twice the magnitude.

Interpreting the zonal dispersal magnitudes shown in Figure 14.9 in terms of advection by a mean flow yields velocities between 0.3 mm/s and 6 mm/s. Except in a few bands of coherent zonal drifts, corresponding in general to regions of high zonal RMS displacements, the tracer trajectories are characterized by both long and short intervals of eastward and westward flows, suggesting a random-walk-like dispersal. This implies that an advective model may not be appropriate for the calculation of dispersal rates. In these cases, the statistics of dispersal can be expressed in terms of an eddy diffusion κ. The units of diffusion are m^2s^{-1} and given a time scale τ, larval lifetime for instance (e.g., Marsh et al. 2001), the distance to which the tracer can diffuse is scaled by $(\kappa\tau)^{1/2}$ as opposed to the linear law which applies to advection by mean flow. The square-root relationship between distance and time implies that in diffusive systems there is a linear relationship between dispersion (as defined in Equation 14.1) and time. In Figure 14.10 this relationship is shown to hold in the South Atlantic after

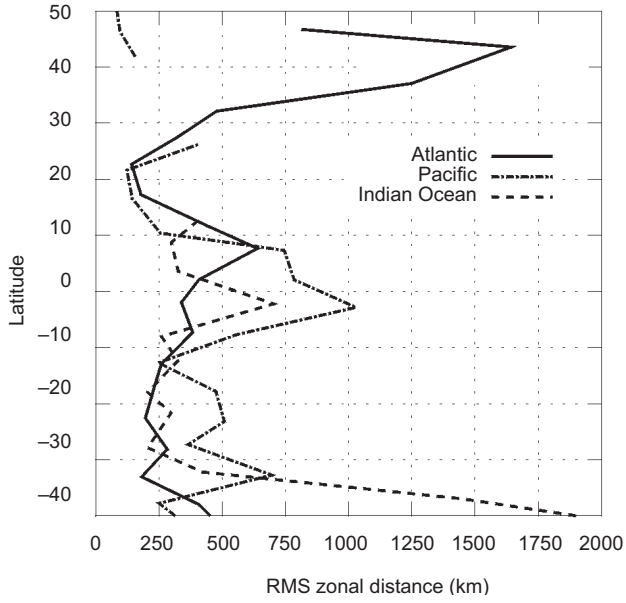

Figure 14.9 RMS zonal dispersal distances in the three major ocean basins, averaged in 5°-latitude bins.

approximately 100 days. Zonal dispersion in other basins has a similar form. Two regimes are classical, an early regime with $d \propto \tau$, and a later, diffusive regime with $d \propto \tau^{1/2}$. The time scale separating the two regimes is roughly the Lagrangian integral time scale, here about 100 days, but in the real ocean at depth more typically of order 10 days (e.g., LaCasce and Speer 1999).

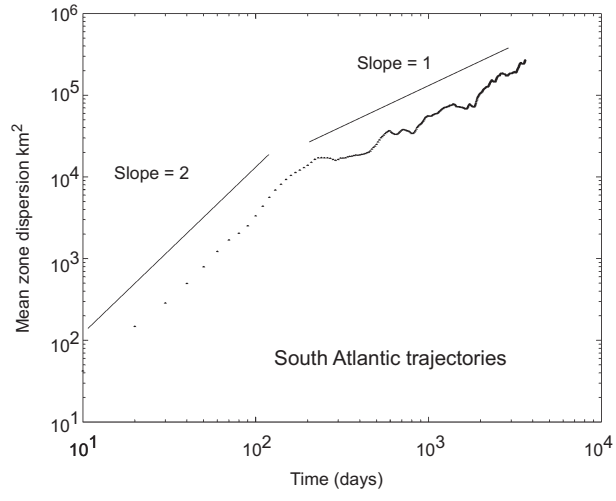

Figure 14.10 Zonal dispersion of simulated trajectories from the South Atlantic Ocean calculated using Equation 14.1.

From the time rate of change of dispersion in the diffusive regime an eddy diffusion can be calculated ($\kappa \approx 500$ m^{2}s^{-1} in the case of Figure 14.9). It should be noted that the velocity, which acts as the constant of proportionality in the early, linear, regime, is an eddy-velocity scale, which is typically greater than the long-term mean velocity.

From the Eurofloat experiment, which is the best data set available for near-ridge dispersion, values for diffusivity were 500–1300 m^{2}s^{-1} over the latitude range 35°–40°N, corresponding to expected 10-year zonal dispersal distances of 400–650 km, approximately half those observed in the same region with the numerical floats (Figure 14.9). A comparison of Figures 14.4 and 14.5 indicates, however, that the Eurofloat trajectories are primarily in the eastern basin, where zonal flows are weak, while the numerical floats show significant drift west of the ridge crest.

These considerations imply that there are regions where tracer dispersal is governed by advection by the mean flow and regions where dispersal is diffusive. So how can we determine the correct scalings to use? Ignoring dispersal shorter than one Lagrangian integral time scale, knowledge of both the mean velocity field and of the mean diffusivity is required to answer that question. Both parameters can be estimated from Lagrangian measurements. In Figure 14.11, typical deep-ocean values have been used to compare the effects of mean-flow advection and eddy diffusion. The mean westward flows in the South Pacific helium plume inferred by Hautala and Riser (1993), for example, range from approximately 2 mm/s to 5 mm/s. The diffusivity in that region is not known but the eddy scales they use in their inverse model (100 km length scale, 5 mm/s velocity scale) implies a value of 500 m^{2}s^{-1}. Figure 14.11 shows that the lower limit of the time scale when off-axis advection by the mean flow becomes important is at least six months and more likely of order two years. This time scale is even longer if the true diffusivity is as high as the one in the Eurofloat region; however, note that along-ridge dispersal by the mean flow is important in the Eurofloat region (Mullineaux

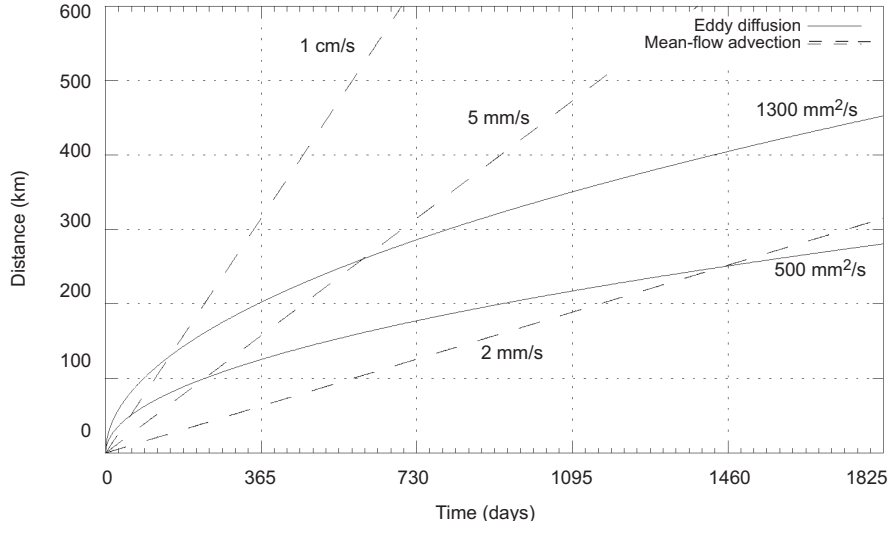

Figure 14.11 Advective versus diffusive dispersion for typical deep oceanic mean flow velocities and eddy diffusivities.

et al. 2002). On time scales between the Lagrangian integral time scale and this mean flow time scale, mean velocities are less relevant to off-ridge dispersal.

CONCLUSION

Lagrangian trajectories from a numerical model of the global ocean circulation have been used to describe dispersion near the MOR crest. In places where comparisons between the model and direct deep velocity data can be made, the model shows similar flow structure, with reduced speeds. Further work comparing the model to observations is in progress. The purpose here is to describe the overall nature of dispersion at the ridge resulting from a variety of physical mechanisms present in the model.

The strong control exerted on circulation by the MOR is apparent in the simulation. Trajectories follow FZs and other small-scale features of the ridge, and are constrained by the overall form of the ridge to flow along it — for great distances in some cases. In other situations, they leave the crest and flow directly into the interior of adjacent basins, carried by wind-driven currents and zonal jets of diverse origins. These phenomena are under investigation in a few regions where experiments have taken place, but much effort is needed to understand dispersion over most of the MOR. Modeling, tracer measurements, including deliberate and natural tracer release experiments, and direct velocity measurement will all be components of such investigations.

Because of the rich spectral properties of oceanic flows dispersal cannot generally be assessed from the mean velocity field alone. Away from strong mean flows, such as boundary currents and the Antarctic Circumpolar Current, the dispersal on time scales of months to years is diffusive in character; estimating the strength of the dispersion is a difficult sampling problem and generally requires Lagrangian measurements.

ACKNOWLEDGMENTS

The Eurofloat data set was collected with the support of the EU MAST II program; ongoing support from IFREMER/LPO for data processing is greatly appreciated. KS and AT are also supported by NSF 9911148 (Deep Basin Experiment Synthesis). Encouragement for this study surfaced at the Census of Marine Life workshop in Woods Hole, spring 2001, especially from F. Grassle.

APPENDIX

The model results used here are from a run of the Parallel Ocean Program (POP) to simulate a five-year period. The model was forced using European Centre for Medium-Range Weather Forecasts (ECMWF) winds, Barnier et al. (1995) surface heat flux, and Levitus (1982) surface salinity restoring on an almost global Mercator grid (78 to 78) with horizontal resolution of 0.28 degrees at the equator (0.06 degrees at 78 and 78) and 20 vertical levels. The model setup is essentially the same as run POP11 as described by Maltrud et al. (1998) with one difference: instead of three-day ECMWF winds, this run uses daily ECMWF winds for the period 1993–1997. Trajectories were calculated with a predictor-corrector time-stepping scheme using ten-day snapshots of the model state linearly interpolated to the current time.

After five years, the trajectories were reinitialized for another five-year period to produce a ten-year trajectory.

REFERENCES

Baker, E.T., J.W. Lavelle, and G.J. Massoth. 1985. Hydrothermal particle plumes over the southern Juan de Fuca Ridge. *Nature* **316**:342–344.

Barnier, B., L. Siefridt, and P. Marchesiello. 1995. Thermal forcing for a global ocean circulation model using a three-year climatology of ECMWF analyses. *J. Mar. Sys.* **6**:363–380.

Davis, R.E. 1991. Observing the general-circulation with floats. *Deep-Sea Res. Part A* **38**:S531–S571 (Suppl. 1).

Hautala, S.L., and S.C. Riser. 1993. A nonconservative β-spiral determination of the deep circulation in the eastern South Pacific. *J. Phys. Oceanogr.* **23**:1975–2000.

Helfrich, K.R., and K.G. Speer. 1995. Oceanic hydrothermal circulation: Mesoscale and basin-scale flow. In: Seafloor Hydrothermal Systems: Physical, Chemical, Biological, and Geological Interactions, ed. S.E. Humphris, R.A. Zierenberg, L.S. Mullineaux, and R.E. Thomson, Geophys. Monograph 91, pp. 347–356. Washington, D.C.: Am. Geophys. Union.

Klinkhammer, G., and A. Hudson. 1986. Dispersal patterns for hydrothermal plumes in the South Pacific using manganese as a tracer. *Earth Planet. Sci. Lett.* **79**:241–249.

LaCasce, J.H. 2000. Floats and f/H. *J. Mar. Res.* **68**:51–95.

LaCasce, J.H., and K.G. Speer. 1999. Lagrangian statistics in unforced barotropic flows. *J. Mar. Res.* **57**:245–274.

Levitus, S. 1982. Climatological Atlas of the World Oceans. NOAA Prof. Paper 13. Washington, D.C.: U.S. Govt. Printing Office.

Lupton, J.E. 1995. Hydrothermal plumes: Near and far field. In: Seafloor Hydrothermal Systems: Physical, Chemical, Biological, and Geological Interactions, ed. S.E. Humphris, R.A. Zierenberg, L.S. Mullineaux, and R.E. Thomson, Geophys. Monograph 91, pp. 347–356. Washington, DC: Am. Geophys. Union.

Lupton, J.E., E.T. Baker, N. Garfield, G.J. Massoth, R.A. Feely, J.P. Cowen, R.R. Greene, and T.A. Rago. 1998. Tracking the evolution of a hydrothermal event plume with a RAFOS neutrally buoyant drifter. *Science* **280**:1052–1055.

Lupton, J.E., and H. Craig. 1981. A major helium-3 source at 15°S on the East Pacific Rise. *Science* **214**:13–18.

Maltrud, M.E., R.D. Smith, A.J. Semtner, and R.C. Malone. 1998. Global eddy-resolving ocean simulations driven by the 1985–1995 atmospheric winds. *J. Geophys. Res.* **103**:30,825–30,853.

Marsh, A.G., L.S. Mullineaux, C.M. Young, and D. Manahan. 2001. Larval dispersal potential of the tubeworm *Riftia pachyptila* at deep-sea hydrothermal vents. *Nature* **411**:77–80.

McDuff, R.E. 1995. Physical dynamics of deep-sea hydrothermal plumes. In: Seafloor Hydrothermal Systems: Physical, Chemical, Biological, and Geological Interactions, ed. S.E. Humphris, R.A. Zierenberg, L.S. Mullineaux, and R.E. Thomson, Geophys. Monograph 91, pp. 347–356. Washington, DC: Am. Geophys. Union.

Mercier, H., and K.G. Speer. 1998. Transport of Antarctic bottom water in the Romanche Fracture Zone and the Chain Fracture Zone. *J. Phys. Oceanogr.* **28**:779–790.

Mullineaux, L.S., K.G. Speer, A.M. Thurnherr, M.E. Maltrud, and A. Vangriesheim. 2002. Implications of cross-axis flow for larval dispersal along mid-ocean ridges. *Cah. Biol. Mar.* **in press. UPDATE??**

Polzin, K.L., J.M. Toole, J.R. Ledwell, and R.W. Schmitt. 1997. Spatial variability of turbulent mixing in the abyssal ocean. *Science* **276**:93–96.

Reid, J.L. 1986. On the total geostrophic circulation of the South Pacific Ocean: Flow patterns, tracers and transports. *Prog. Oceanogr.* **16**:1–61.

Rüth, C., R. Well, and W. Roether. 2000. Primordial ^{3}He in South Atlantic deep waters from sources on the Mid-Atlantic Ridge. *Deep-Sea Res. I* **47**:1059–1075.

Speer, K.G. 1998. A new spin on hydrothermal plumes. *Science* **280**:1034–1035.
Speer, K.G., J. Gould, and J. LaCasce. 1999. Year-long float trajectories in the Labrador Sea Water of the eastern North Atlantic Ocean. *Deep-Sea Res. II* **46**:165–179.
Speer, K.G., and K.R. Helfrich. 1995. Hydrothermal plumes: A review of flow and fluxes. In: Hydrothermal Vents and Processes, ed. L.M. Parson, C.L. Walker, and D.R. Dixon, pp. 373–386. London: Geol. Soc.
Stramma, L. 1992. The South Indian Ocean Current. *J. Phys. Oceanogr.* **22**:421–430.
Thurnherr, A.M., K.J. Richards, C.R. German, G.F. Lane-Serff, and K.G. Speer. 2002. Flow and mixing in the rift valley of the Mid-Atlantic Ridge. *J. Phys. Oceanogr.* **32**:1763–1778
Treguier, A.-M., N.G. Hogg, M. Maltrud, K.G. Speer, and V. Thierry. 2002. On the origin of deep zonal flows in the Brazil Basin. *J. Phys. Oceanogr.*, **submitted. UPDATE??**